Molecular Cell 22, 807–818, June 23, 2006 ©2006 Elsevier Inc. DOI 10.1016/j.molcel.2006.04.026

Is Dimerization Required for the Catalytic Activity of Bacterial Biotin Carboxylase?

Yang Shen,[1] Chi-Yuan Chou,[2] Gu-Gang Chang,[2] and Liang Tong[1,*]
[1] Department of Biological Sciences
Columbia University
New York, New York 10027
[2] Faculty of Life Sciences
National Yang-Ming University
Taipei 112
Taiwan

Summary

Acetyl-coenzyme A carboxylases (ACCs) have crucial roles in fatty acid metabolism. The biotin carboxylase (BC) subunit of *Escherichia coli* ACC is believed to be active only as a dimer, although the crystal structure shows that the active site of each monomer is 25 Å from the dimer interface. We report here biochemical, biophysical, and structural characterizations of BC carrying single-site mutations in the dimer interface. Our studies demonstrate that two of the mutants, R19E and E23R, are monomeric in solution but have only a 3-fold loss in catalytic activity. The crystal structures of the E23R and F363A mutants show that they can still form the correct dimer at high concentrations. Our data suggest that dimerization is not an absolute requirement for the catalytic activity of the *E. coli* BC subunit, and we propose a new model for the molecular mechanism of action for BC in multisubunit and multidomain ACCs.

Introduction

ACCs play pivotal roles in fatty acid metabolism (Cronan and Waldrop, 2002; Munday, 2002; Tong, 2005; Wakil et al., 1983). They catalyze the carboxylation of acetyl-coenzyme A (acetyl-CoA) to produce malonyl-CoA, which is the first and rate-limiting step in fatty acid biosynthesis (Cronan and Waldrop, 2002). The malonyl-CoA product is also a potent inhibitor of fatty acid oxidation in animals (Abu-Elheiga et al., 2001; McGarry and Brown, 1997). ACCs are attractive targets for the developments of new drugs against many human diseases (such as diabetes, obesity, and bacterial and fungal infections) (Harwood, 2004; Lenhard and Gottschalk, 2002; Tong, 2005). ACC inhibitors have been used as herbicides in agriculture for more than 20 years (Devine and Shukla, 2000; Gronwald, 1991; Sasaki and Nagano, 2004).

ACCs are found in most living organisms, from bacteria to humans. ACCs from prokaryotes and the plastids of most plants are multisubunit enzyme complexes (Cronan and Waldrop, 2002; Sasaki and Nagano, 2004; Tong, 2005). They are composed of a BC subunit, a biotin carboxyl carrier protein (BCCP) subunit, and two proteins (α and β) for the carboxyltransferase (CT) subunit. The BC activity catalyzes the carboxylation of biotin from bicarbonate, which is coupled with the hydrolysis of ATP. The biotin prosthetic group is covalently linked to the BCCP subunit. The CT activity transfers the activated carboxyl group from carboxybiotin to acetyl-CoA to generate the malonyl-CoA product.

In comparison, ACCs from most eukaryotes are large, multidomain enzymes, with molecular weights of about 250 kDa (Munday, 2002; Tong, 2005; Wakil et al., 1983). Domains in these enzymes can be identified that share sequence homology with the subunits of the prokaryotic ACCs. For example, the BC domain of yeast ACC has 35% sequence identity to the BC subunit of *E. coli* ACC. On the other hand, the sequence conservation between the CT domains of eukaryotic ACCs and the CT subunits of bacterial ACCs is significantly lower (around 10%).

The *E. coli* BC subunit has been used as a model for studying the BC activity of ACCs and other biotin-dependent carboxylases. This subunit is catalytically active when isolated from the other ACC subunits and can use free biotin as the substrate (Guchhait et al., 1974). Moreover, the crystal structure of this enzyme has been available for more than 10 years (Waldrop et al., 1994). BC belongs to the ATP-grasp superfamily of enzymes (Artymiuk et al., 1996) and consists of three domains: A, B, and C (Figure 1A). The B domain is highly flexible in structure in the free enzyme and undergoes a large conformational change upon ATP binding to help close the active site for catalysis (Thoden et al., 2000). The recent structures of the BC domain of yeast ACC (Shen et al., 2004) as well as the BC subunit of *Aquifex aeolicus* pyruvate carboxylase (Kondo et al., 2004) share similar features.

The *E. coli* BC subunit is a dimer in solution and in the crystal (Figure 1A) (Guchhait et al., 1974; Thoden et al., 2000; Waldrop et al., 1994), and a similar dimer is observed in the crystal of the BC subunit of *Aquifex aeolicus* pyruvate carboxylase (Kondo et al., 2004). Monomeric forms of the *E. coli* BC subunit can only be observed under denaturing conditions (Janiyani et al., 2001), suggesting that the dimer may be stable.

It is currently believed that *E. coli* BC is active only as a dimer, whereas monomers of the enzyme are presumed to be inactive catalytically (Janiyani et al., 2001). The strongest evidence comes from studies on hybrid dimers of the BC subunits, where one monomer is wild-type and the other carries an inactivating mutation in the active site (Janiyani et al., 2001). The catalytic activity of such hybrid dimers is only about 2% of that of the wild-type dimer, suggesting that there may be communication between the two active sites of the dimer (although the *E. coli* BC subunit does not exhibit cooperativity). Additional evidence comes from observations on isolated eukaryotic BC domains (Shen et al., 2004; Weatherly et al., 2004). They are monomeric in solution and catalytically inactive, which appears to be consistent with the dimerization requirement. However, the molecular basis for this requirement is not known. The structure shows that the active site in each monomer is about 25 Å away from the dimer interface in the bacterial BC subunit, with no direct contribution from residues

*Correspondence: tong@como.bio.columbia.edu

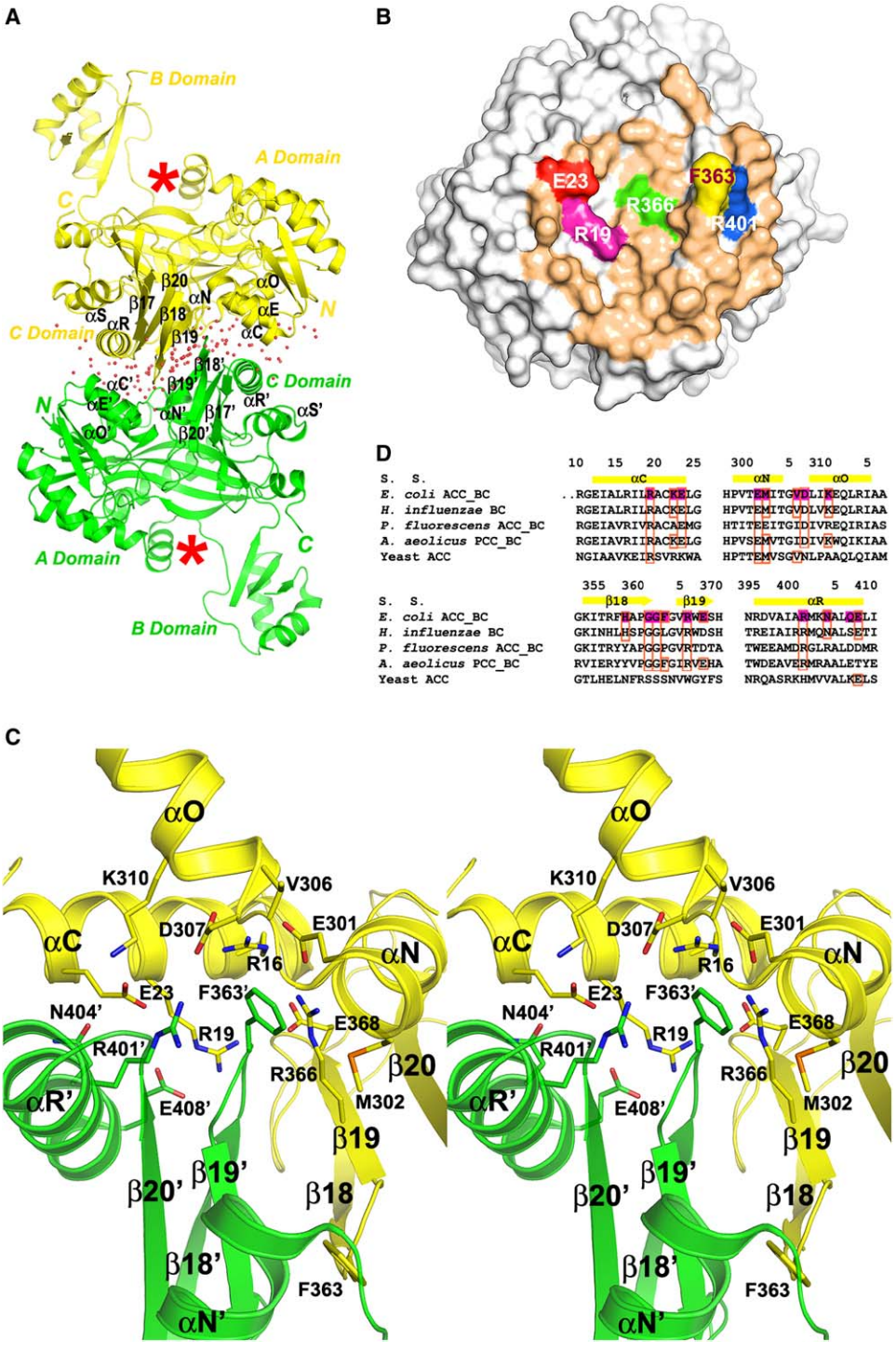

Figure 1. Structure of *E. coli* BC Subunit

(A) Schematic drawing of the free enzyme dimer of wild-type *E. coli* BC subunit (Thoden et al., 2000; Waldrop et al., 1994). One monomer is shown in yellow, and the other is in green. The red stars indicate the two active sites of the enzyme. Water molecules in the dimer interface are shown as red dots. Please see Figure S1 for the stereo version of this figure.

(B) Molecular surface of the BC subunit. Residues in the dimer interface are colored tan, and those selected for mutagenesis are highlighted.

(C) Stereo drawing showing detailed interactions in the dimer interface. The prime symbol indicates residues and secondary structures from the second monomer. Water molecules have been omitted for clarity. Produced with Pymol (DeLano, 2002).

(D) Sequence alignment of dimer interface regions of the BC subunits of *E. coli*, *H. influenzae*, *P. fluorescens*, *A. aeolicus*, and the BC domain of yeast ACC. Residues in the *E. coli* BC dimer interface are highlighted in magenta.

in the other monomer of the dimer (Figure 1A). The molecular mechanism for the long-range communication between the two active sites in this dimer remains to be elucidated.

None of the experiments so far directly measured the catalytic activity of the monomeric form of the *E. coli* BC subunit. To assess whether dimerization is really required for the catalytic activity of this enzyme, we have generated monomeric forms of the BC subunit by introducing single-point mutations in the dimer interface. Sedimentation velocity analytical ultracentrifugation experiments showed that the mutations produced up to 8000-fold increase in the K_d of the dimer, such that the mutants are essentially monomeric in solution. Our kinetic studies, however, showed that these mutants still have robust catalytic activity, in fact only 3-fold weaker than that of the wild-type enzyme. To reveal the molecular basis for the destabilization of the dimer by the mutations, we have determined the crystal structures of the E23R and F363A mutants at up to 2.2 Å resolution. Overall, our biochemical, biophysical, and structural analyses suggest that, contrary to current beliefs, dimerization is not absolutely required for the catalytic activity of the *E. coli* BC subunit. Based on these data, we propose a new model for the molecular mechanism of action of biotin carboxylase.

Results and Discussion

Selection of Residues in the Dimer Interface for Mutagenesis

The BC subunit of *E. coli* ACC exists as dimers both in solution and in the crystal (Figure 1A, and see Figure S1 available in the Supplemental Data with this article online) (Guchhait et al., 1974; Thoden et al., 2000; Waldrop et al., 1994). About 1270 $Å^2$ of the surface area of each monomer is buried at the dimer interface (Figure 1B), consistent with the belief that the dimer may be stable (Janiyani et al., 2001). Surprisingly, however, the BC dimer interface is rather hydrophilic in nature. Most of the residues at the interface are charged (Figure 1C), and there are more than 100 water molecules in the interface based on the crystal structure of the BC subunit at high resolution (Figure 1A) (Thoden et al., 2000).

Dimerization of the BC subunit involves the interactions of the β hairpin containing strands β18 and β19 with their symmetry mates related by the 2-fold axis of the dimer (Figure 1A). In addition, helix αR from one monomer contacts helices αC′ and αE′ of the other monomer (with the prime indicating the second monomer) (Figure 1A). The charged residues in this interface include the ion pairs between Arg19 and Glu23 in one monomer with residues Glu408′ and Arg401′ in the other monomer, respectively (Figure 1C). Phe363 makes the largest contribution to the buried surface area in the dimer (about 150 $Å^2$), but its side chain is mostly in contact with two ion pairs (Arg16′–Asp307′ and Glu301′–Arg366′) in the other monomer (Figure 1C).

A sequence comparison indicates that Arg19 is identical among all BCs of biotin-dependent enzymes (Figure 1D), suggesting a conserved and crucial role for this residue at the dimer interface. Glu23, Arg366, and Arg401 are identical among bacterial BC subunits but are not conserved in the yeast BC domain (Figure 1D). Phe363 is poorly conserved even among bacterial BC subunits (Figure 1D), which may be consistent with the fact that this side chain is not specifically recognized in the dimer interface (Figure 1C).

Based on the structural and sequence analyses, we designed the following six mutations in the dimer interface: R19E, E23R, F363W, F363A, R366E, and R401E (Figure 1B). The mutations will introduce the opposite charge in the side chains of residues 19, 23, 366, and 401, which should disrupt the ion pair interactions for these residues in the dimer interface. For the Phe363 residue, the mutations will either increase (Trp) or decrease (Ala) the bulk of the side chain, which could also be detrimental to the dimerization of the BC subunit.

Dimer Interface Mutants Are Monomeric in Solution

Wild-type and mutant BC subunits were overexpressed in *E. coli* and purified by nickel affinity and gel filtration chromatography. The expression levels of the His-tagged, recombinant BC proteins are significantly higher than that of the untagged, endogenous *E. coli* BC subunit (Figure S2). Therefore, contamination of the purified recombinant BC samples by endogenous wild-type BC subunit is expected to be minimal. This is also confirmed by our structural analysis on the F363A mutant (see below).

The gel filtration studies showed that the wild-type (with MW of 50 kDa for the monomer) and the F363W mutant of BC eluted at 69.5 ml from an S-300 column, corresponding to the dimeric form of the enzyme. In comparison, the R19E, F363A, E23R, and R366E mutants eluted at a volume of 73 ml, suggesting that these mutants may be monomeric instead. Approximately 30% of the E23R and R366E protein eluted at the void volume (38 ml), whereas the R401E mutant predominantly eluted as a soluble aggregate at around 40 ml.

To obtain further evidence for the monomeric behavior of the dimer interface mutants, we characterized the oligomerization state of these mutants and the wild-type protein by static light scattering. Wild-type BC exists exclusively as a dimer in solution, with an observed molecular weight (MW) of 87 kDa based on light scattering. Consistent with the gel filtration results, the R19E, E23R, F363A, and R366E mutants have MWs from 43–48 kDa, corresponding to a monomeric state of these proteins in solution. Interestingly, an MW of 58 kDa was observed for the F363W mutant, suggesting an equilibrium between monomer and dimer for this mutant. The lower protein concentration in the light scattering studies (3 μM) as compared to the gel filtration studies (60 μM) may account for the difference in oligomerization state for this mutant. Overall, our gel filtration and light scattering studies show that we have successfully created monomeric BC subunits by introducing single-site mutations in the dimer interface.

Dramatic Increases in the K_d through Mutations in the Dimer Interface

To validate our observations from the gel filtration and light scattering studies and to obtain quantitative measurements for the effects of the mutations on the monomer-dimer equilibrium, we performed sedimentation velocity analytical ultracentrifugation (AUC) studies on the wild-type and mutant BCs. The experiments were

Table 1. K_d of Wild-Type and Mutant *E. coli* BC Subunits

Protein	100 mM HEPES (pH 8.0), 8 mM $MgCl_2$	+ 40 mM Biotin	+ 0.4 mM ATP	+ 40 mM Biotin, + 0.4 mM ATP
Wild-type	0.160 ± 0.008	0.039 ± 0.001	0.276 ± 0.002	0.097 ± 0.001
R19E	703 ± 38	404 ± 18	208 ± 2	843 ± 7
E23R	598 ± 30	302 ± 39	255 ± 1	540 ± 6
F363A	4.5 ± 0.2	27.5 ± 0.6	3.3 ± 0.01	4.0 ± 0.04

The K_d values are given in micrometers. They were derived from a global fit to the sedimentation velocity AUC data, obtained at three different protein concentrations of 1.0, 6.1, and 41 μM.

performed in a buffer that is essentially identical to that used in kinetic assays on these proteins, 100 mM HEPES (pH 8.0), 8 mM $MgCl_2$, 40 mM biotin, and 0.4 mM ATP (Table 1). Therefore, our AUC data on these proteins are directly relevant to the analysis of their kinetic data (see next). To assess whether substrate binding can affect the stability of the dimer, we also performed the AUC experiments in buffers lacking biotin, ATP, or both substrates (Table 1). Earlier experiments have shown that the biotin substrate can synergistically increase the rate of ATP hydrolysis upon binding to the enzyme (Blanchard et al., 1999; Thoden et al., 2000).

The sedimentation velocity AUC data for wild-type BC and the R19E, E23R, and F363A mutants can be readily fit to a monomer-dimer rapid self-association model (Figure 2 and Figure S3), and the K_d values for these proteins were derived from this fit (Table 1). In the presence of both biotin and ATP, the K_d for the wild-type BC dimer is about 0.1 μM, consistent with earlier data suggesting that this dimer is rather stable in solution (Janiyani et al., 2001). In comparison, the K_d values for the mutants are dramatically higher than those for the wild-type enzyme. The largest increase in K_d is seen for the R19E mutant (up to 8700-fold), in agreement with its strong conservation (Figure 1D). In comparison, the F363A mutant shows a more moderate increase (about 40-fold), and this residue is poorly conserved (Figure 1D). There is about 5-fold variation in the K_d values for each protein in the absence of ATP and/or biotin (Table 1), suggesting that the BC dimer is not stabilized by substrate binding in the conditions that we tested.

The significantly increased K_d values for the R19E and E23R mutants (500–800 μM) explain our observation of predominantly monomeric forms of these two mutants in the gel filtration and light scattering studies, where 3–60 μM of enzymes were used. The K_d for the F363A mutant is between 3 and 28 μM based on our sedimentation velocity data (Table 1). At 3 μM concentration of F363A, we would expect to have roughly a 1:1 ratio of monomer and dimer species. However, in the light scattering assay, F363A is only a monomer (48 kDa) at such a concentration. This could be due to the differences between the buffers used for light scattering (20 mM Tris [pH 8.5] and 100 mM NaCl) and AUC studies.

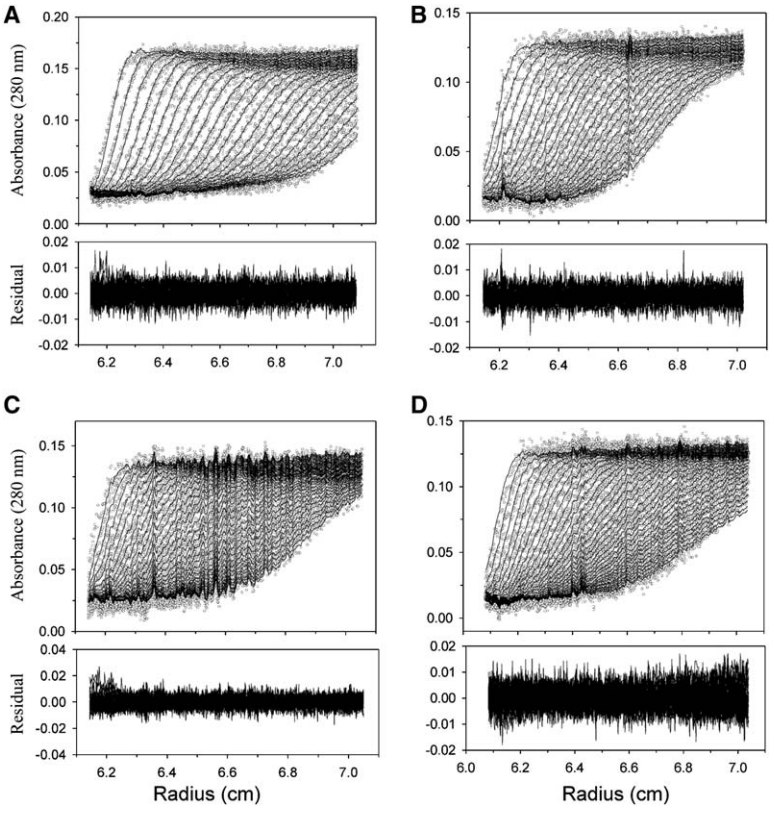

Figure 2. Sedimentation Velocity Analytical Ultracentrifugation Data for the BC Subunit

The observed spectrum (open circles) and the fit to the data based on the monomer-dimer rapid self-association model (lines) for the wild-type (A), R19E (B), E23R (C), and F363A (D) mutants of *E. coli* BC subunit. The protein concentration was at 6.1 μM, and the buffer contained 100 mM HEPES (pH 8.0) and 8 mM $MgCl_2$. The root-mean-square deviation of all the fits was below 0.01, indicating high-quality data and fitting (Schuck, 2003). For plots from the other two concentrations (1.0 and 41 μM), please see Figure S3.

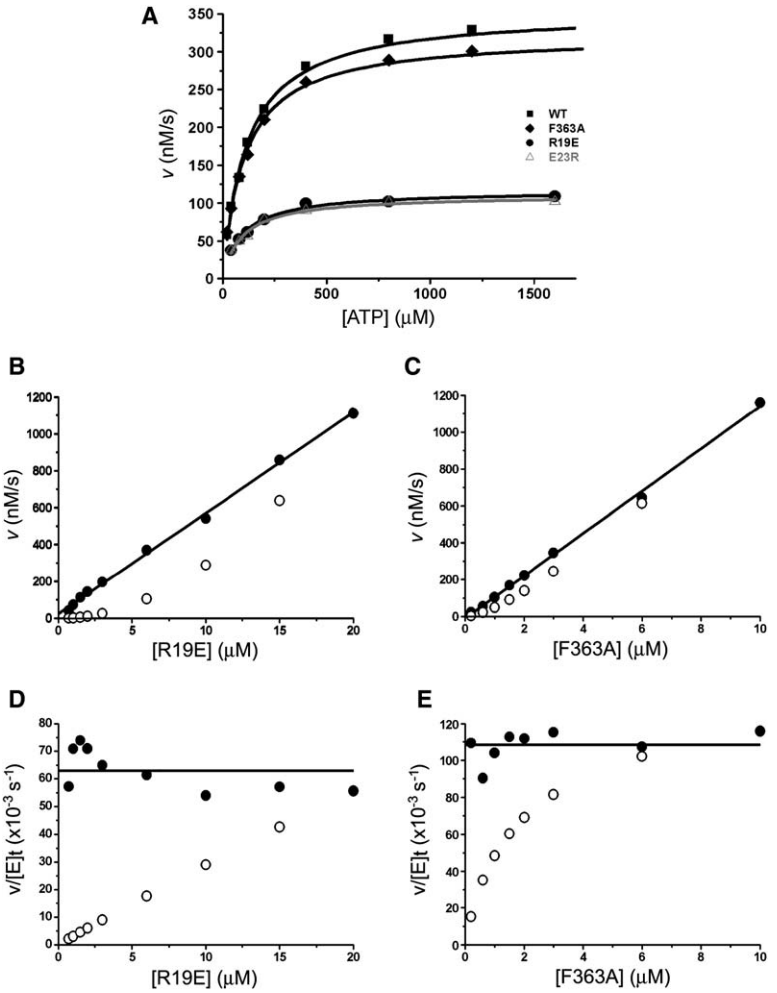

Figure 3. Catalytic Activity of *E. coli* BC Subunit

(A) Plot of the initial reaction velocity as a function of the substrate (ATP) concentration for wild-type, R19E, E23R, and F363A mutants. The assay monitored the biotin-dependent ATP hydrolysis reaction of the BC subunit. The concentration of the enzyme was at 2.5 μM.

(B) Dependence of the initial velocity of the R19E mutant on enzyme concentration (filled circles). The straight line represents a fit to the data assuming monomers are active. The open circles are the theoretical values if the dimer is the only active species, using the K_d value observed by the AUC experiment (Table 1).

(C) Dependence of the initial velocity of the F363A mutant on enzyme concentration.

(D) Plot of the specific activity ($v/[E]_t$) of the R19E mutant as a function of enzyme concentration (filled circles). The open circles show the theoretical values if the dimer is the only active species.

(E) Plot of the specific activity of the F363A mutant as a function of enzyme concentration.

The AUC data for the R401E and R366E mutants could not be fit to the monomer-dimer rapid self-association model (data not shown). This is consistent with our gel filtration and light scattering studies, which showed that these two mutants have a strong tendency to form aggregates.

The Dimer Interface Mutants Are Catalytically Active as Monomers

Our gel filtration, light scattering, and AUC studies show that the R19E and E23R mutants are monomeric in solution and that the F363A mutant exists in a monomer-dimer equilibrium at micromolar concentrations. We next sought to characterize the catalytic properties of these mutants. The kinetic assays monitored the biotin-dependent hydrolysis of ATP, and the concentration of the wild-type and mutant enzymes was at 2.5 μM in each reaction. Based on our observed K_d values (Table 1), if dimerization of the BC subunits is required for activity, we would expect the R19E and E23R mutants to be essentially inactive, whereas the F363A mutant should have about 50% of the activity of the wild-type enzyme.

Contrary to these expectations, we found that all three mutants have robust catalytic activity (Figure 3A). In fact, the R19E and E23R mutants have only a 3-fold loss in k_{cat}, whereas their K_m for ATP is essentially the same as the wild-type BC (Table 2). The F363A mutant has the same catalytic activity as the wild-type enzyme (Table 2). The observed activity for these mutants is unlikely due to contamination from the endogenous wild-type *E. coli* BC subunit; the strongest evidence showing that there is little such contamination comes from our structural studies on the F363A mutant (see below). Therefore, our kinetic data demonstrate that the R19E and E23R mutants of *E. coli* BC are active in their monomeric form.

Because our data contradict current belief regarding the catalytic activity of BC, we performed additional experiments to verify that monomers of the mutants are truly active. These experiments examined the dependence of the initial velocity (v) of the reaction on the total

Table 2. Kinetic Parameters for Biotin-Dependent ATP Hydrolysis

Enzyme	K_m for ATP (μM)	k_{cat} (s^{-1})	k_{cat}/K_m (s^{-1} M^{-1})
Wild-type	115.2 ± 8.2	0.228 ± 0.004	1980 ± 120
R19E	94.8 ± 8.7	0.075 ± 0.002	790 ± 60
E23R	93.0 ± 10.0	0.071 ± 0.002	760 ± 70
F363A	104.9 ± 6.4	0.207 ± 0.003	1980 ± 100
R366E[a]	–	–	–
R401E[a]	–	–	–

[a] No specific activity was observed at 2.5 μM of enzyme and up to 800 μM of ATP.

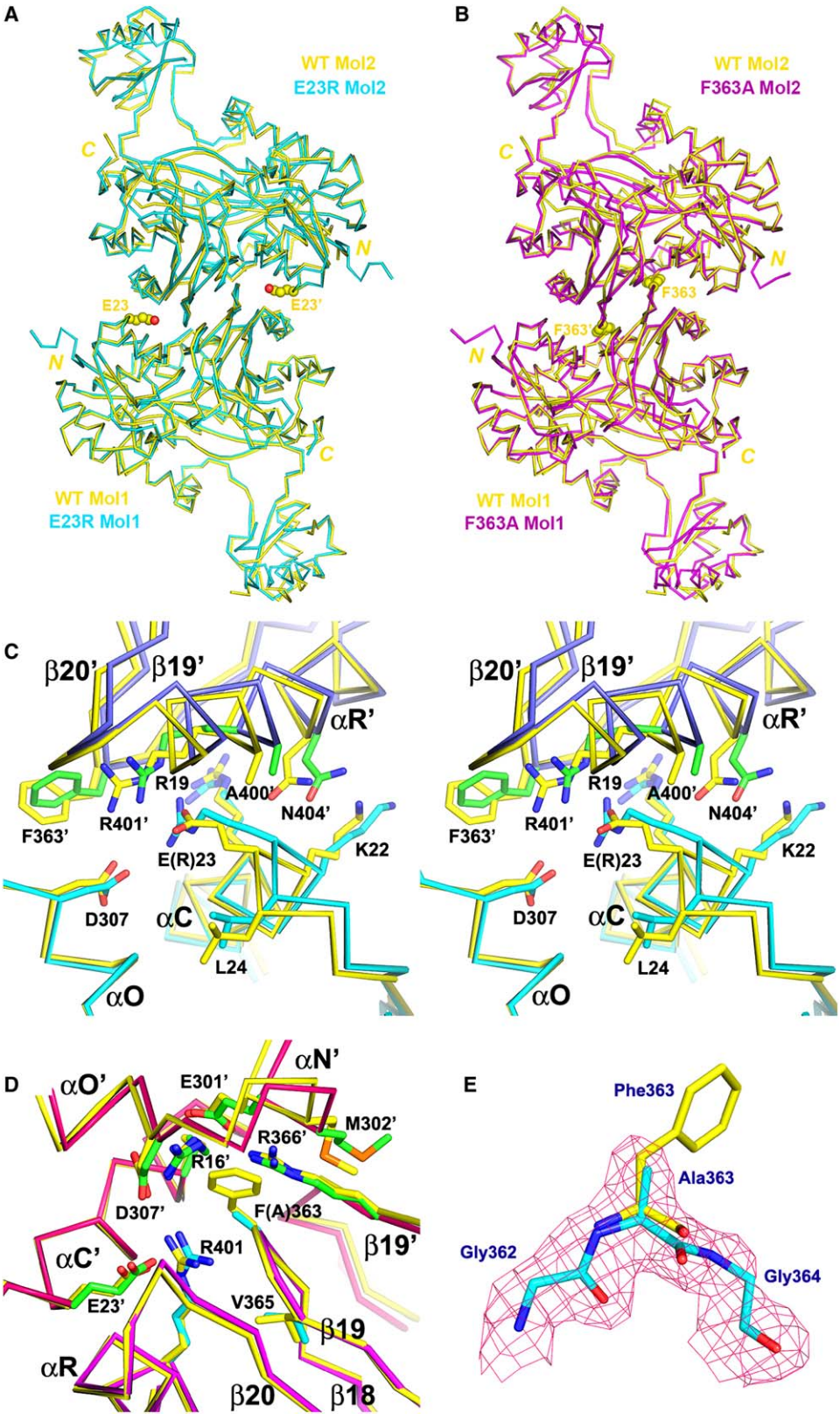

Figure 4. Crystal Structures of the E23R and F363A Mutants of *E. coli* BC Subunit

(A) Overlay of the structures of the E23R mutant (in cyan) and the wild-type BC (in yellow). Only one of the monomers (Mol1) is used for the superposition between the two structures.

(B) Overlay of the structures of the F363A mutant (in magenta) and the wild-type BC (in yellow).

(C) Stereo plot showing structural differences between the E23R mutant and the wild-type BC near the mutation site.

concentration of the enzyme, $[E]_t$, at saturating concentrations of the substrates (2 mM ATP). If monomers of the enzyme are as active as the dimer, a linear dependence is expected,

$$v = k_{cat}[E]_t$$

where $[E]_t$ is given in terms of the monomer. However, if the enzyme is only active in the dimeric form, a nonlinear dependence is expected,

$$v = k_{cat}\left(K_d + 4[E]_t - \sqrt{K_d^2 + 8K_d[E]_t}\right)/8.$$

Our experimental data for the R19E (concentration range 0.7–20 μM) and F363A (0.2–10 μM) mutants are consistent with a linear dependence of the initial velocity on enzyme concentration, whereas the nonlinear model does not fit the data (Figures 3B and 3C). The difference between the two models is even more dramatic if the specific activity (v / $[E]_t$) is plotted against $[E]_t$. The linear model will produce a horizontal line, at the k_{cat}, whereas the nonlinear model will produce a curve starting at 0. Our experimental data for the R19E and F363A mutants can be readily fit to a horizontal line (Figures 3D and 3E). It is notable that the difference between the linear and nonlinear plots is more significant for the R19E mutant than the F363A mutant, due to the higher K_d of the former. In summary, both of our kinetic experiments demonstrate that monomers of mutant BC are essentially fully active in the assays.

This concentration-dependence assay unfortunately cannot be applied directly to the wild-type BC subunit to determine whether its monomers are active. Because of the low K_d value of the dimer (97 nM, Table 1), much lower concentrations of the enzyme (around 1–10 nM) must be used in the reaction. However, the initial velocity cannot be measured accurately at such enzyme concentrations. In addition, it has been suggested that the wild-type BC dimers are stable in solution and rarely dissociate (Janiyani et al., 2001).

The R366E and R401E mutants are inactive, with no specific activity at ATP concentrations of up to 800 μM (Table 2). Noting that these two mutants are also prone to aggregation, it is likely that the R366E and R401E mutations have disrupted the native structure of the BC subunit.

Structural Disruptions in the Dimer Interface of the E23R Mutant

Our biochemical, biophysical, and kinetic studies show that the R19E and E23R mutations of *E. coli* BC have severely destabilized the dimer of the enzyme, with more than an 8000-fold increase in the K_d values (Table 1), but the monomers of these mutants are active catalytically (Table 2). In comparison, the F363A mutation caused a smaller increase in the K_d of the dimer (Table 1), and the mutant has essentially the same activity as the wild-type enzyme (Table 2). To elucidate the molecular basis for the effects of the mutations on the dimerization of these enzymes, we have determined the crystal structures of the E23R and F363A mutants at 2.8 and 2.2 Å resolution, respectively (Table 3). Attempts at crystallizing the R19E mutant have so far not been successful.

Table 3. Summary of Crystallographic Information

Structure	E23R	F363A
Resolution range (Å)	30–2.8	30–2.2
Number of observations	71,292	234,905
R_{merge}[a] (%)	6.4 (30.0)	10.9 (24.6)
I/σI	16.2 (3.1)	8.5 (4.5)
Observation redundancy	3.0 (2.6)	2.9 (2.5)
Number of reflections	21,174	78,337
Completeness (%)	94 (76)	88 (73)
R factor[b] (%)	20.1 (33.9)	19.2 (22.1)
Free R factor[b] (%)	26.0 (49.7)	25.0 (30.2)
rms deviation in bond lengths (Å)	0.013	0.006
rms deviation in bond angles (°)	1.5	1.3

[a] $R_{merge} = \sum_h \sum_i |I_{hi} - \langle I_h \rangle| / \sum_h \sum_i I_{hi}$. The numbers in parentheses are for the highest resolution shell.
[b] $R = \sum_h |F_h^o - F_h^c| / \sum_h F_h^o$.

The E23R and the F363A mutants are dimeric in the crystal (Figures 4A and 4B). This could be expected as very high concentrations of both mutants (300 μM for E23R and 180 μM for F363A) were used in the crystallization, which is close to the K_d of the E23R mutant and is significantly greater than the K_d of the F363A mutant (Table 1). There are two dimers of the F363A mutant in the crystallographic asymmetric unit. They have essentially the same conformations, with a root-mean-square (rms) distance of 0.4 Å for 879 equivalent Cα atoms. The E23R crystal is nonisomorphous to the F363A crystal and contains only one dimer in the asymmetric unit. The monomers of the mutants have essentially the same overall conformation as the wild-type BC monomer, with rms distances of about 0.4 Å for equivalent Cα atoms between any pair of the monomers. Residues in the B domain (amino acids 132–202), far from the dimer interface (Figure 1A), are not included in this comparison. This domain shows variations among the structures (Figures 4A and 4B), but these are more likely due to the inherent flexibility of the domain and crystal packing effects.

There are significant changes in the structure of the *E. coli* BC subunit near the E23R mutation site (Figure 4C), which are likely triggered by the E23R mutation itself. Residues 22–27 at the end of the αC helix moved by about 1 Å to accommodate the larger Arg23 side chain, which may have affected the position of the N terminus of helix αR', including Ala400′ and Asn404′ (Figure 4C). The mutation destroyed the ion-pair interaction between Glu23 and Arg401′. The guanidinium group of the new Arg23 side chain is instead interacting with the side chain of Asp307, in the same monomer, and the Arg401′ side chain is disturbed by the new positive charge. The side chain of Phe363′ assumes a different rotamer in this monomer (Figure 4C), although that of Phe363 in the other

(D) Structural differences between the F363A mutant and the wild-type BC near the mutation site.
(E) Final $2F_o - F_c$ electron density map (in magenta) for residues 362–364 of the F363A mutant (in cyan) at 2.2 Å resolution. The Phe363 residue in the wild-type BC is also shown (in yellow). The contour level is at 1σ. Produced with Pymol (DeLano, 2002).

monomer has the same conformation as the wild-type enzyme. This suggests that the Phe363 may have become somewhat more flexible in the E23R mutant.

There are also differences in the dimer organization of the E23R mutant compared to the wild-type BC (Figure 4A). If one monomer of the E23R mutant is superimposed onto that of the wild-type-free enzyme, a rotation of 3.5° is needed to bring the second monomers of the two structures into superposition. However, it is not clear whether these changes are due to the E23R mutation or the flexibility in the dimer interface. As a comparison, a 2° difference is seen in the orientation of the second monomer of the E288K mutant (in the active site) in complex with ATP (Thoden et al., 2000).

The F363A mutant shows a 5° rotation of the second monomer but roughly in the opposite direction relative to the E23R mutant (Figure 4B). Aside from this difference in dimer organization, the F363A mutant does not show significant structural changes near the mutation site (Figure 4D).

Our structural studies with the E23R and F363A mutants show that the E23R mutation produces significant conformational changes near the mutation site in the dimer interface, consistent with the large increase in the K_d of this mutant dimer. On the other hand, only minor structural changes are observed for the F363A mutant, and the loss of the van der Waals interactions of the Phe363 side chain may be the molecular basis for the moderate increase in the K_d of this mutant dimer.

The availability of high-resolution X-ray diffraction data for the F363A mutant also allowed us to quantitatively assess the amount of contamination by endogenous, wild-type *E. coli* BC subunit in our enzyme preparations. As the mutant proteins were strongly overexpressed compared to the endogenous BC subunit (Figure S2), significant contamination by the endogenous enzyme is unlikely. Our crystallographic analysis for the F363A mutant shows that there is no evidence for any electron density beyond the Cβ atom of this side chain (Figure 4E). Similarly, clear electron density was observed for the Arg23 side chain in the E23R mutant (Figure S4). This is an independent confirmation that our protein preparations have a negligible amount of the endogenous, wild-type BC, and the observed catalytic activity of these mutants (Table 2) is not due to this contamination. Our analyses cannot exclude the possibility that only the mutant proteins crystallized in our experiments while the contaminating wild-type protein (if there was any) stayed in solution, although such a scenario is probably unlikely.

Implications for the BC Subunit of Multisubunit ACCs

It is currently believed that *E. coli* BC is active only as a dimer. However, the only experimental evidence is obtained from studies on hybrid dimers containing a wild-type monomer and a monomer with a disabled active site (Janiyani et al., 2001). These studies suggest there might be long-range communication between the two active sites in the dimer, and catalysis in the two active sites may be coupled (Janiyani et al., 2001). A possible mechanism is that the two subunits alternate their catalytic cycles, such that only one subunit is turning over the substrate at a time while the other subunit goes through product release and substrate binding (Janiyani et al., 2001). With this model, if catalysis in one active site is disrupted (for example by mutation), catalysis in the other active site will also be affected severely, thereby explaining the large loss in activity of the hybrid dimers (Janiyani et al., 2001).

Although studies on the hybrid dimers of the BC subunit suggest possible communication between the two active sites of the dimer, they do not directly address the issue whether monomers of the BC subunit are catalytically active. Our new data demonstrate that the R19E and E23R mutants are monomeric in solution but have strong catalytic activity, showing that monomers of the BC subunit can be catalytically active. However, our data do not necessarily contradict the earlier observations on the hybrid dimers (Janiyani et al., 2001). Although communication may be important in the dimer form of the enzyme, it apparently is not required for catalysis and the monomer form of the enzyme can also be active. Therefore, dimerization may not be an absolute requirement for the catalytic activity of the BC subunit of multisubunit ACCs. Further studies are needed to elucidate how events in one active site of the dimer are transmitted across the dimer interface to the other active site.

The BC subunit functions in a multisubunit complex with BCCP and CT in prokaryotic ACCs. The bacterial CT subunit and the yeast CT domain are tightly associated dimers, with the active sites located in the dimer interface (Bilder et al., 2006; Tong, 2005; Zhang et al., 2003, 2004b). Therefore, CT is only active as a dimer, and it is likely to remain dimeric in the multisubunit ACCs. The BC subunit is probably also dimeric in this holoenzyme, considering the fact the *E. coli* BC dimers are stable (Table 1) and slow to dissociate (Janiyani et al., 2001). Interestingly, the distance between the two active sites of the BC dimer is about the same as that between the two active sites of the CT dimer. This suggests a possible model for the holoenzyme where the BC dimer has direct interactions with the CT dimer, which could position the two active sites in BC close to those in CT. The biotin substrate, attached to a swinging arm on BCCP, can then translocate between the BC and CT active sites. Each pair of the BC:CT active sites may be in contact with two BCCP subunits in the holoenzyme (Choi-Rhee and Cronan, 2003).

Implications for the BC Domain of Multidomain ACCs: A New Model for the Activity of BC

The BC domains of multidomain ACCs from human and yeast have been studied recently (Shen et al., 2004; Weatherly et al., 2004). It was found that these isolated domains are catalytically inactive, in contrast to observations that the carboxyltransferase (CT) domains of human and yeast ACCs are active (Tong, 2005; Zhang et al., 2004a; Zhang et al., 2003). The BC domains are monomeric in solution, which appears to be consistent with the belief that only BC dimers are active. However, with our new data on the dimer interface mutants, the monomeric behavior of the BC domains may not be the only explanation for their lack of catalytic activity.

Although the overall structures of the *E. coli* BC subunit (Thoden et al., 2000; Waldrop et al., 1994) and yeast BC domain (Shen et al., 2004) are similar, there are significant differences for the residues in the dimer interface of *E. coli* BC (Shen et al., 2004). In fact, a model for

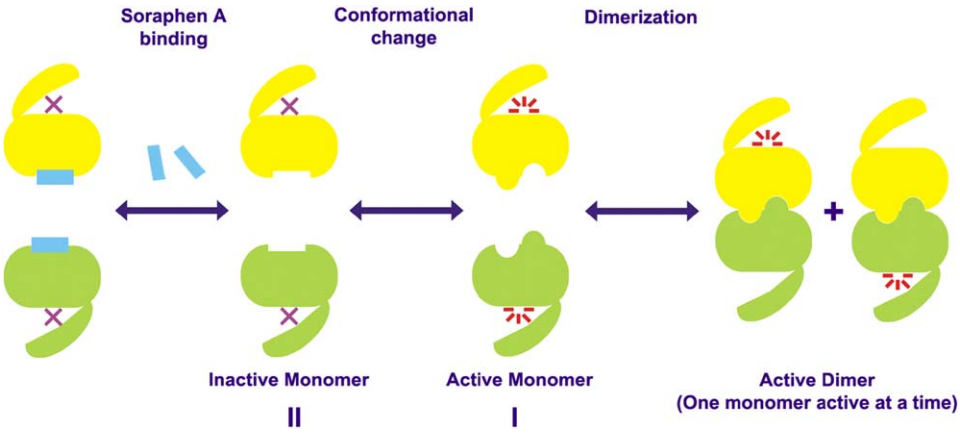

Figure 5. A Model for the Mechanism of Action of BC

Residues in the dimer interface can assume two states (conformations I and II). Conformation I, found in bacterial BC subunits, is compatible with dimerization and catalysis. Conformation II, found in isolated BC domains of multidomain ACCs, is incompatible with dimerization and catalysis. Soraphen A binds and stabilizes this inactive state of the multidomain BC enzyme.

the dimer of the yeast BC domain shows severe steric clashes in the interface (Figure S5). The largest difference is that strand β18 is located in completely different positions in the two structures (Figure 1A and Figure S5), and this strand in yeast BC domain is clashing with its symmetry mate from the other monomer in the dimer model (Figure S5). Another structural difference is that the position of strand β19 shifts by about 3 Å between the two enzymes (Shen et al., 2004). Remarkably, these conformational differences are crucial for the formation of the binding site for the natural product soraphen A and the specificity of this compound for eukaryotic ACCs (Shen et al., 2004). Our earlier studies showed that this potent polyketide inhibitor stabilizes the monomeric form of the BC domain, consistent with the hypothesis that its binding site may mediate dimerization (or oligomerization) of the BC domain.

Based on our data on the dimer interface mutants and existing information on the BC subunits and BC domains, we propose a new model for the molecular mechanism of action of these enzymes (Figure 5). The model proposes that residues in the dimer interface can assume two (or more) conformations that can indirectly control catalysis in the active site of the enzyme (Janiyani et al., 2001). The conformation of these residues in wild-type *E. coli* BC subunit (conformation I) is compatible with dimerization of the enzyme (Figure 5). However, the catalytic activity of the two monomers in the dimer may be coupled, such that only one monomer is turning over the substrate at a time (Figure 5) (Janiyani et al., 2001). Our single-site mutations in the dimer interface can severely destabilize the dimers, but they do not seriously perturb the conformation of the residues in the dimer interface, such that the proper dimer can still be formed at high concentrations (Figures 4A and 4B). Monomers of these dimer interface mutants are catalytically active (Figure 5), suggesting that long-range communication between the two active sites of the dimer can be decoupled.

In contrast, residues in the dimer interface of the yeast BC domain assume a different conformation (conformation II) (Figure 5). It is incompatible with dimerization of the BC domain (Figure S5), and the enzyme in this state is catalytically inactive (Figure 5). We hypothesize that a change to conformation I for these residues is needed to make the eukaryotic BC domain active (Figure 5). This is expected to occur in the native context of the BC domain in the full-length multidomain ACC enzyme; whether isolated BC domain can achieve this conformational transition remains to be seen. The natural product soraphen A binds and stabilizes the inactive state (conformation II) of the enzyme (Figure 5), inhibiting protein-protein interactions between BC domain monomers (Shen et al., 2004). Therefore, our model suggests that the conformation of the residues in the dimer interface may be more important than dimerization itself for the catalytic activity of these enzymes and that dimerization per se is not an absolute requirement for the function of biotin carboxylase.

Moreover, our model suggests the possibility that the catalytically active conformation of the BC domain (conformation I) does not have to form dimers, as the monomeric BC in this conformation can also be active (Figure 5). BC is covalently linked to the BCCP and CT domains in the eukaryotic ACCs, which exist as homo-oligomers. Although it is likely that the BC domain is dimeric in this multidomain holoenzyme, it might also be possible that BC is present in the monomer form, and the active conformation interacts instead with other domains of the enzyme. In fact, our preliminary observations (based on cryo-electron microscopy) on the related enzyme propionyl-CoA carboxylase (PCC) show that the α subunit (containing BC and BCCP) might be arranged as monomers around a central hexameric core of β subunits (containing CT) (Y.S., B. Deng, H. Zhou, L.T., unpublished data). The structure of this hexameric core has been determined by crystallographic methods (Diacovich et al., 2004; Hall et al., 2003; Lin et al., 2006). Therefore, our model could be applicable not only to ACC but also to other biotin-dependent carboxylases. This further strengthens our finding that dimerization is not an absolute requirement for BC activity.

In summary, our studies provide experimental evidence that *E. coli* BC subunit can function catalytically in its monomeric form, contrary to current beliefs. By

introducing single-site mutations in the dimer interface, we have been able to produce two mutants (R19E and E23R) that are monomeric in solution at micromolar concentrations. However, these mutants have only a 3-fold loss in activity compared to the wild-type enzyme. Crystal structures of the E23R and the F363A mutants reveal the molecular mechanism for the destabilizing effects of these mutations on the BC dimer. Our biochemical, biophysical, and structural studies have significant functional implications for the BC subunit of bacterial ACCs as well as the BC domain of multidomain, eukaryotic ACCs.

Experimental Procedures

Mutagenesis, Protein Expression, and Purification

Full-length wild-type *E. coli* BC was subcloned into the pET28a vector (Novagen). The expression construct contains an N-terminal hexa-histidine tag. Six mutants (R19E, E23R, F363W, F363A, R366E, and R401E) were designed based on the structural information on the BC dimer. They were created by using the QuikChange kit (Stratagene) and verified by DNA sequencing of the mutated plasmid.

The wild-type and mutant BC proteins were overexpressed in *E. coli* Rosetta (DE3) cells and purified following the same protocol, with nickel-agarose and gel filtration chromatography. The purified proteins were concentrated to 10–50 mg/ml in a buffer containing 20 mM Tris (pH 8.5), 200 mM NaCl, 8 mM DTT, and 5% (v/v) glycerol, flash-frozen in liquid nitrogen, and stored at −80ºC. The purity of these samples is >95% based on SDS gel electrophoresis.

Sedimentation Velocity Analytical Ultracentrifugation

Sedimentation velocity experiments were performed with a Beckman model XL-A analytical ultracentrifuge for four protein samples, wild-type, R19E, E23R, and F363A, in the same buffer as that used for kinetic assay. The protein samples were first diluted to concentrations of 1.0, 6.1, and 41 μM, respectively. Samples (400 μl) and reference (440 μl) solutions were loaded into double-sector centerpieces and mounted in a Beckman An-50 Ti rotor. The reference solution contained 40 mM biotin and/or 0.4 mM ATP as necessary. The experiments were performed at 20ºC with a rotor speed of 42,000 rpm. Absorbance of the sample at 280 nm was monitored in a continuous mode without averaging, using a time interval of 480 s and step size of 0.002 cm.

Multiple scans at different time points were globally fitted to a monomer-dimer rapid self-association model by using the program SEDPHAT (Schuck, 2003). The isotherm of the weight-average sedimentation coefficient for a self associating system can be written as

$$s_w(c_{tot}) = \sum_i \frac{s_{0,i}}{1 + k_{s,i} K_i c_1^i} K_i c_1^i / c_{tot} \cong \frac{1}{1 + k_s c_{tot}} \sum_i s_{0,i} K_i c_1^i / c_{tot}$$

where $s_{0,i}$ are the species sedimentation coefficients at infinite dilution, $k_{s,i}$ are their hydrodynamic nonideality coefficients, and K_i is the association constant ($K_1 = 1$). Because the values of $k_{s,i}$ cannot be easily determined separately for each species and may be composition dependent, the second equation makes the assumption that the hydrodynamic nonideality coefficients for all species can, in a first approximation, be described by an average value (Frigon and Timasheff, 1975). This will be true at moderate concentrations, or if the different species are not too dissimilar in shape, or for moderately weak associations where the largest species dominate the sedimentation at higher concentration.

For rapid associating systems, finite element solutions of the Lamm equation

$$\frac{\partial c}{\partial t} = -\frac{1}{r}\left(\frac{\partial}{\partial r}\left(s_w(c(r))\omega^2 r^2 c - D_g(c(r)) r \frac{\partial c}{\partial r}\right)\right)$$

with local weight-average sedimentation coefficients s_w and gradient-average diffusion coefficients D_g were calculated as described previously (Cox, 1969; Schuck, 1998; Schuck, 2003). In the equation, r denotes the distance from the center of rotation, ω is the angular velocity, and c is the concentration. For Lamm equation solutions with hydrodynamic repulsive nonideality, the local weight-average sedimentation coefficients were multiplied with a factor of 1 / (1 + $k_s c(r)$), as described previously (Schuck, 2003; Solovyova et al., 2001). In SEDPHAT, to generate a global model, a set of sedimentation profiles is calculated by using the monomer-dimer model for each channel. Global parameters are s_{20} (sedimentation coefficient at 20ºC), D_{20} (diffusion constant at 20ºC), log K_a (association constants), M (molar mass) values, and the partial-specific volume of the solute. Local parameters are the protein concentration of each sedimentation profiles. Among the global parameters, the s_{20}, M of monomer, and log K_a are varied to obtain the best fit to the data.

Kinetic Studies

The initial velocity of ATP hydrolysis of the wild-type and mutant enzymes of *E. coli* BC was determined spectrophotometrically at 340 nm, following a protocol described earlier (Blanchard et al., 1999). The reaction buffer (0.2 ml volume) contained 100 mM HEPES (pH 8.0), 15 mM $KHCO_3$, 8 mM $MgCl_2$, 40 mM biotin, 0.2 mM NADH, 0.5 mM phosphoenolpyruvate, 7 units of lactate dehydrogenase, and 4.2 units of pyruvate kinase (40 mM biotin was solubilized by vigorous mixing and incubation at 37ºC). The concentration of the ATP substrate was varied in the assays. The measurements were repeated two to three times for each enzyme.

The dependence of BC catalytic activity on enzyme concentration was investigated by using the R19E and F363A mutants, at 2 mM ATP concentration. The initial velocity of the reaction at various concentrations of each mutant enzyme was determined.

Crystallization of the E23R and F363A Mutants

The hexa-histidine tag was not removed from the mutants for crystallization. Crystals of the E23R mutant were obtained at 21ºC by the sitting-drop vapor diffusion method. The protein was at 15 mg/ml concentration, mixed in a 1:0.7 ratio with a reservoir solution containing 0.1 M magnesium formate, 14% (w/v) PEG3350, 8% (v/v) glycerol, and 20 mM $CaCl_2$. Microseeding was required to obtain crystals of diffraction quality, and the crystals took 20–30 days to grow to full size. For cryo protection, the crystals were transferred to a solution containing 0.1 M magnesium formate, 25% (w/v) PEG3350, and 16% (v/v) glycerol and flash-frozen in liquid propane for data collection at 100K. They belong to space group $P2_1$ with cell parameters of a = 62.9 Å, b = 92.6 Å, c = 86.6 Å, and β = 98.8º. There are two molecules of the mutant in the asymmetric unit.

Crystals of the F363A mutant were obtained at 21ºC by the sitting-drop vapor diffusion method. The protein was at 9 mg/ml concentration, mixed at a ratio of 1.6:1 with a reservoir solution containing 0.1 M Bis-Tris (pH 7.5), 100 mM NaCl, 200 mM trimethylamine N-oxide, 8% (w/v) PEG2000 MME, 4% (v/v) glycerol, 5 mM $MgCl_2$, and 2.5 mM DTT. These crystals were cryo protected in the reservoir solution supplemented to 22% PEG2000 MME and 14% glycerol. They belong to space group $P2_1$ with cell parameters a = 62.4 Å, b = 81.5 Å, c = 176.6 Å, and β = 97.7º. There are four molecules of the mutant in the asymmetric unit. These mutant crystals are not isomorphous to those of the wild-type BC (Waldrop et al., 1994).

Data Collection and Structure Determination

X-ray diffraction data on the E23R and F363A mutants were collected on the ADSC Quantum-4 CCD at beamline X4A and ADSC Q315 CCD at beamline X29 of National Synchrotron Light Source (NSLS), respectively. The diffraction images were processed and scaled with the HKL package (Otwinowski and Minor, 1997).

The structures of the E23R and F363A mutants were determined by the molecular replacement method with the program COMO (Jogl et al., 2001), using the structure of the free enzyme of wild-type *E. coli* BC as a search model (Thoden et al., 2000). The structure refinement was performed with the program CNS (Brunger et al., 1998) and manual adjustments to the model with the program O (Jones et al., 1991). For the E23R mutant, NCS restraint was applied during the structure refinement, and TLS refinement was used in the final step with the program Refmac5 (Murshudov et al., 1997). The crystallographic information is summarized in Table 3.

Supplemental Data

Supplemental Data include five figures and can be found with this article online at http://www.molecule.org/cgi/content/full/22/6/807/DC1/.

Acknowledgments

We thank Randy Abramowitz and John Schwanof for setting up the beamline at X4A; Howard Robinson for setting the beamline at X29; and Song Xiang, Michael Rudolph, Thierry Auperin, and Yun Bai for help with data collection. This research is supported in part by a grant from the National Institutes of Health (DK67238) to L.T.

Received: January 29, 2006
Revised: March 27, 2006
Accepted: April 20, 2006
Published: June 22, 2006

References

Abu-Elheiga, L., Matzuk, M.M., Abo-Hashema, K.A.H., and Wakil, S.J. (2001). Continuous fatty acid oxidation and reduced fat storage in mice lacking acetyl-CoA carboxylase 2. Science *291*, 2613–2616.

Artymiuk, P.J., Poirrette, A.R., Rice, D.W., and Willett, P. (1996). Biotin carboxylase comes into the fold. Nat. Struct. Biol. *3*, 128–132.

Bilder, P., Lightle, S., Bainbridge, G., Ohren, J., Finzel, B., Sun, F., Holley, S., Al-Kassim, L., Spessard, C., Melnick, M., et al. (2006). The structure of the carboxyltransferase component of acetyl-CoA carboxylase reveals a zinc-binding motif unique to the bacterial enzyme. Biochemistry *45*, 1712–1722.

Blanchard, C.Z., Lee, Y.M., Frantom, P.A., and Waldrop, G.L. (1999). Mutations at four active site residues of biotin carboxylase abolish substrate-induced synergism by biotin. Biochemistry *38*, 3393–3400.

Brunger, A.T., Adams, P.D., Clore, G.M., DeLano, W.L., Gros, P., Grosse-Kunstleve, R.W., Jiang, J.-S., Kuszewski, J., Nilges, M., Pannu, N.S., et al. (1998). Crystallography & NMR system: a new software suite for macromolecular structure determination. Acta Crystallogr. D. Biol. Crystallogr. *54*, 905–921.

Choi-Rhee, E., and Cronan, J.E., Jr. (2003). The biotin carboxylase-biotin carboxyl carrier protein complex of Escherichia coli acetyl-CoA carboxylase. J. Biol. Chem. *278*, 30806–30812.

Cox, D. (1969). Computer simulation of sedimentation in the ultracentrifuge. IV. Velocity sedimentation of self-associating solutes. Arch. Biochem. Biophys. *129*, 106–123.

Cronan, J.E., Jr., and Waldrop, G.L. (2002). Multi-subunit acetyl-CoA carboxylases. Prog. Lipid Res. *41*, 407–435.

DeLano, W.L. (2002). The PyMOL Manual (San Carlos, CA: DeLano Scientific).

Devine, M.D., and Shukla, A. (2000). Altered target sites as a mechanism of herbicide resistance. Crop Prot. *19*, 881–889.

Diacovich, L., Mitchell, D.L., Pham, H., Gago, G., Melgar, M.M., Khosla, C., Gramajo, H., and Tsai, S.-C. (2004). Crystal structure of the b-subunit of acyl-CoA carboxylase: structure-based engineering of substrate specificity. Biochemistry *43*, 14027–14036.

Frigon, R.P., and Timasheff, S.N. (1975). Magnesium-induced self-association of calf brain tubulin. II. Thermodynamics. Biochemistry *14*, 4567–4573.

Gronwald, J.W. (1991). Lipid biosynthesis inhibitors. Weed Sci. *39*, 435–449.

Guchhait, R.B., Polakis, S.E., Dimroth, P., Stoll, E., Moss, J., and Lane, M.D. (1974). Acetyl coenzyme A carboxylase system from Escherichia coli. Purification and properties of the biotin carboxylase, carboxyltransferase, and carboxyl carrier protein components. J. Biol. Chem. *249*, 6633–6645.

Hall, P.R., Wang, Y.-F., Rivera-Hainaj, R.E., Zheng, X., Pustai-Carey, M., Carey, P.R., and Yee, V.C. (2003). Transcarboxylase 12S crystal structure: hexamer assembly and substrate binding to a multienzyme core. EMBO J. *22*, 2334–2347.

Harwood, H.J., Jr. (2004). Acetyl-CoA carboxylase inhibition for the treatment of metabolic syndrome. Curr. Opin. Investig. Drugs *5*, 283–289.

Janiyani, K., Bordelon, T., Waldrop, G.L., and Cronan, J.E., Jr. (2001). Function of Escherichia coli biotin carboxylase requires catalytic activity of both subunits of the homodimer. J. Biol. Chem. *276*, 29864–29870.

Jogl, G., Tao, X., Xu, Y., and Tong, L. (2001). COMO: a program for combined molecular replacement. Acta Crystallogr. *D57*, 1127–1134.

Jones, T.A., Zou, J.Y., Cowan, S.W., and Kjeldgaard, M. (1991). Improved methods for building protein models in electron density maps and the location of errors in these models. Acta Crystallogr. *A47*, 110–119.

Kondo, S., Nakajima, Y., Sugio, S., Yong-Biao, J., Sueda, S., and Kondo, H. (2004). Structure of the biotin carboxylase subunit of pyruvate carboxylase from Aquifex aeolicus at 2.2 Å resolution. Acta Crystallogr. D. Biol. Crystallogr. *60*, 486–492.

Lenhard, J.M., and Gottschalk, W.K. (2002). Preclinical developments in type 2 diabetes. Adv. Drug Deliv. Rev. *54*, 1199–1212.

Lin, T.W., Melgar, M.M., Kurth, D., Swamidass, S.J., Purdon, J., Tseng, T., Gago, G., Baldi, P., Gramajo, H., and Tsai, S.-C. (2006). Structure-based inhibitor design of AccD5, an essential acyl-CoA carboxylase carboxyltransferase domain of Mycobacterium tuberculosis. Proc. Natl. Acad. Sci. USA *103*, 3072–3077.

McGarry, J.D., and Brown, N.F. (1997). The mitochondrial carnitine palmitoyltransferase system. From concept to molecular analysis. Eur. J. Biochem. *244*, 1–14.

Munday, M.R. (2002). Regulation of mammalian acetyl-CoA carboxylase. Biochem. Soc. Trans. *30*, 1059–1064.

Murshudov, G.N., Vagin, A.A., and Dodson, E.J. (1997). Refinement of macromolecular structures by the maximum-likelihood method. Acta Crystallogr. *D53*, 240–255.

Otwinowski, Z., and Minor, W. (1997). Processing of X-ray diffraction data collected in oscillation mode. Methods Enzymol. *276*, 307–326.

Sasaki, Y., and Nagano, Y. (2004). Plant acetyl-CoA carboxylase: structure, biosynthesis, regulation, and gene manipulation for plant breeding. Biosci. Biotechnol. Biochem. *68*, 1175–1184.

Schuck, P. (1998). Sedimentation analysis of noninteracting and self-associating solutes using numerical solutions to the Lamm equation. Biophys. J. *75*, 1503–1512.

Schuck, P. (2003). On the analysis of protein self-association by sedimentation velocity analytical ultracentrifugation. Anal. Biochem. *320*, 104–124.

Shen, Y., Volrath, S.L., Weatherly, S.C., Elich, T.D., and Tong, L. (2004). A mechanism for the potent inhibition of eukaryotic acetyl-coenzyme A carboxylase by soraphen A, a macrocyclic polyketide natural product. Mol. Cell *16*, 881–891.

Solovyova, A., Schuck, P., Costenaro, L., and Ebel, C. (2001). Non-ideality by sedimentation velocity of halophilic malate dehydrogenase in complex solvents. Biophys. J. *81*, 1868–1880.

Thoden, J.B., Blanchard, C.Z., Holden, H.M., and Waldrop, G.L. (2000). Movement of the biotin carboxylase B-domain as a result of ATP binding. J. Biol. Chem. *275*, 16183–16190.

Tong, L. (2005). Acetyl-coenzyme A carboxylase: crucial metabolic enzyme and attractive target for drug discovery. Cell. Mol. Life Sci. *62*, 1784–1803.

Wakil, S.J., Stoops, J.K., and Joshi, V.C. (1983). Fatty acid synthesis and its regulation. Annu. Rev. Biochem. *52*, 537–579.

Waldrop, G.L., Rayment, I., and Holden, H.M. (1994). Three-dimensional structure of the biotin carboxylase subunit of acetyl-CoA carboxylase. Biochemistry *33*, 10249–10256.

Weatherly, S.C., Volrath, S.L., and Elich, T.D. (2004). Expression and characterization of recombinant fungal acetyl-CoA carboxylase and isolation of a soraphen-binding domain. Biochem. J. *380*, 105–110.

Zhang, H., Yang, Z., Shen, Y., and Tong, L. (2003). Crystal structure of the carboxyltransferase domain of acetyl-coenzyme A carboxylase. Science *299*, 2064–2067.

Zhang, H., Tweel, B., Li, J., and Tong, L. (2004a). Crystal structure of the carboxyltransferase domain of acetyl-coenzyme A carboxylase in complex with CP-640186. Structure *12*, 1683–1691.

Zhang, H., Tweel, B., and Tong, L. (2004b). Molecular basis for the inhibition of the carboxyltransferase domain of acetyl-coenzyme A carboxylase by haloxyfop and diclofop. Proc. Natl. Acad. Sci. USA *101*, 5910–5915.

Accession Numbers

The atomic coordinates have been deposited at the Protein Data Bank under ID codes 2GPS and 2GPW.